58. W. G. Harrison *et al.*, *J. Plankton Res.* **9**, 235 (1987).
59. W. J. Jenkins, *Nature* **331**, 521 (1988).
60. A particularly important comparison will be between the subtropical zone, where nutrient input is believed to be episodic, and the equatorial zone, where the nutrient supply is more persistent through upwelling. To do the integrations over time, the variance at seasonal and shorter time scales must be known.
61. A. F. Vezina and T. Platt, *Can. J. Fish. Aquat. Sci.* **44**, 198 (1987).
62. F. C. Fuglister, *Atlantic Ocean Atlas* (Woods Hole Oceanographic Institution, Woods Hole, MA, 1960).
63. F. E. Muller-Karger, C. R. Mclain, P. L. Richardson, *Nature* **333**, 56 (1988).
64. This work was supported by a grant-in-aid from the Department of Ocean Development (New Delhi) to the National Institute of Oceanography (Goa). Collaboration was facilitated by the award of a Natural Science and Engineering Research Council (NSERC) of Canada International Scientific Exchange Award to S.S. Further NSERC support through an operating grant to T.P. is gratefully acknowledged. We thank N. Kuring and C. Caverhill for help with computations and R. T. Barber, W. G. Harrison, E. P. W. Horne, M. R. Lewis, and A. R. Longhurst for useful comments.

Fractal Reaction Kinetics

RAOUL KOPELMAN

Classical reaction kinetics has been found to be unsatisfactory when the reactants are spatially constrained on the microscopic level by either walls, phase boundaries, or force fields. Recently discovered theories of heterogeneous reaction kinetics have dramatic consequences, such as fractal orders for elementary reactions, self-ordering and self-unmixing of reactants, and rate coefficients with temporal "memories." The new theories were needed to explain the results of experiments and supercomputer simulations of reactions that were confined to low dimensions or fractal dimensions or both. Among the practical examples of "fractal-like kinetics" are chemical reactions in pores of membranes, excitation trapping in molecular aggregates, exciton fusion in composite materials, and charge recombination in colloids and clouds.

AMONG THE MOST IMPORTANT CHEMICAL REACTIONS ARE those called "heterogeneous." These reactions take place at interfaces of different phases, for example, gas-solid or liquid-solid boundaries, and include reactions such as industrial surface-catalysis and electrode reactions, as well as many bioenzymatic and membrane reactions and some geochemical and atmospheric reactions. In addition, there are many heterogeneous "nonchemical" reactions: in solid-state physics there are electron-hole, soliton-antisoliton, and exciton-exciton "recombinations," as well as the aggregation of excitations, defects, and so forth. Charge and excitation recombination, as well as excitation quenching, are also found in biological systems, such as photosynthetic units.

The most universally found instruction in chemical synthesis is to "stir well." However, convective stirring cannot always be achieved for reactions in or on media that are solid, viscous, porous, or otherwise structured. In the absence of convective stirring, there is still diffusive stirring, which is called "self-stirring." However, under dimensional constraints (surface reactions) or topological constraints (solid-state reactions), self-stirring may be highly inefficient. Fractal spaces such as percolation clusters are ideal testing grounds for "understirred" reaction kinetics. However, a reaction medium does not have to be a geometrical fractal in order to exhibit fractal kinetics. The drastic and unexpected consequences of such "fractal-like reaction kinetics" are described below.

Classical Kinetics

Classical, homogeneous chemical kinetics will be briefly reviewed so as to introduce the terminology of fractal kinetics. We limit ourselves to elementary (single-step) bimolecular (pairwise) reactions, as these are by far the most important and prevalent chemical (and nonchemical) reactions. For a single-reactant bimolecular reaction,

$$A + A \rightarrow \text{products} \quad (1)$$

as well as for a two-reactant bimolecular reaction,

$$A + B \rightarrow \text{products} \quad (2)$$

one has second-order reaction rates, that is, all of the concentration dependence of the reaction can be expressed either as

$$\text{Rate} = K[A]^2 \quad (A + A \rightarrow A) \quad (3)$$

or as

$$\text{Rate} = K[A][B] \quad (A + B \rightarrow 0) \quad (4)$$

where [A] is the reactant concentration (or density) of A and K is the rate constant (not to be confused here with the equilibrium constant). Note that K is independent of time. Equations 3 and 4 are valid for both "batch" and "steady-state" conditions. In the batch case, the system is prepared instantaneously (at time $t = 0$), and the reaction rate is given by

$$\text{Rate} = -d[A]/dt = -d[B]/dt \quad (5)$$

that is, the disappearance of reactant concentration per unit time. Substituting Eq. 5 into Eq. 3 or 4 gives a differential rate equation:

$$-d[A]/dt = K[A]^2 \quad (A + A \rightarrow A) \quad (3a)$$

Its solution (the integrated rate equation) is:

$$[A]^{-1} - [A_0]^{-1} = Kt \quad (6)$$

where $[A_0]$ is the initial concentration (at $t = 0$). Similarly

$$-d[A]/dt = K[A][B] \quad (A + B \rightarrow 0) \quad (4a)$$

If [A] = [B], Eq. 6 is also the solution of Eq. 4a.

The author is professor of chemistry at the Department of Chemistry, University of Michigan, Ann Arbor, MI 48109.

However, at "steady state" the reactants are supplied at the same rate R at which they are consumed. The most general case is given by

$$d[A]/dt = R - K[A]^2 \quad (7)$$

Here $d[A]/dt$ is the instantaneous net change in [A], which is given by the difference between the rate of production R and the rate of reaction $K[A]^2$. Again, Eq. 7 is valid for A + B if [A] = [B] and $R_A = R_B$. Note that one can start ($t = 0$) with $[A_0] = [B_0] = 0$ and $R_A = R_B$ (constant in time). The reaction will then follow Eq. 7 until a steady state is reached ($d[A]/dt = 0$), at which time Eq. 7 reduces to Eq. 3. In both batch and steady-state reactions, it is assumed that changes in concentration with time do not affect chemical reactivity.

At the turn of the century, Smoluchowski (*1*) showed that for self-stirred (diffusion-limited) homogeneous reactions in three-dimensional (3-D) systems, $K \sim D$, that is, the rate constant is linearly proportional to the "diffusion constant" D. Both D and K are time independent. Although Smoluchowski's derivation implied that the above is not true for lower dimensions, this result was recognized explicitly only in recent years (*2–4*).

Fractal-Like Kinetics

In classical kinetics, we do not expect the rate constant K to have any time dependence. However, experimental studies on the reaction kinetics of excitons in molecular macro-clusters (inside crystalline isotopic alloys) that were prepared as fractals yielded very anomalous results in which rate constants depend on time (*4, 5*). These reactions are believed to have simple mechanisms and it is also easy to monitor the instantaneous concentrations of both reactants and products. Specifically, it is an exciton-fusion reaction, where two triplet (T) excitations fuse and form a singlet (S) excitation:

$$T + T \rightarrow S \quad (8)$$

Both reactant and product are "radioactive" in the sense that both are metastable and that radiation is one of the decay products (green light from T and ultraviolet from S). In analogy to radioactive tracers, the concentration can be monitored as a function of time (for both reactant and product). This reaction is diffusion limited. In perfect crystals it behaves classically according to Eqs. 3, 3a, and 7. However, in isotopically mixed crystals the reaction shows the above-mentioned anomalies. Following Eq. 3a, one can plot K versus time (Fig. 1). For isotopic alloys well above the critical mole fraction (see below), one obtains a time-independent curve (top curve of Fig. 1). For alloy mole fractions near or below the critical value, one obtains the time-dependent curve (bottom, Fig. 1). In the log-log plot the slope ($-h$) is a constant in all cases. When $h = 0$, K is time-independent; however, when $h \neq 0$, K is time-dependent at all times. To emphasize this time dependence, K is replaced by $k \sim t^{-h}$ and

$$\log k = -h \log t + \text{constant} \quad (9)$$

The excitons are confined to one isotopic species ($C_{10}H_8$). In the ideal solid solution ($C_{10}H_8/C_{10}D_8$) the molecules of one species (say $C_{10}H_8$) are distributed randomly among the lattice sites. The critical mole fraction is the lowest isotopic composition for which the excitons are able to diffuse ("percolate") throughout the sample. At lower mole fractions, each exciton is trapped within a small $C_{10}H_8$ cluster, and the exciton fusion reaction is inefficient. At the "critical" composition the $C_{10}H_8$ molecules form a macroscopic cluster that extends throughout the crystal. Such a loosely connected extended cluster (Fig. 2) is called a "percolation cluster," and is a textbook example (*6, 7*) of a "fractal." For this fractal, $h = 1/3$ (see below).

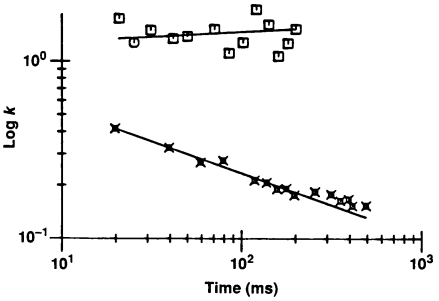

Fig. 1. Log-log plot of instantaneous rate constant k versus time t, for the exciton fusion reaction (Eq. 8) in isotopically mixed naphthalene crystals [see (*4*)] at the critical percolation composition (bottom curve) and well above it (top curve). The analysis of this experiment (*4, 5*) gave $h = 0.32 \pm 0.03$ for the bottom curve (compared with the theoretical value of 0.33) and $h = 0.03$ for the top curve (theoretical value of 0).

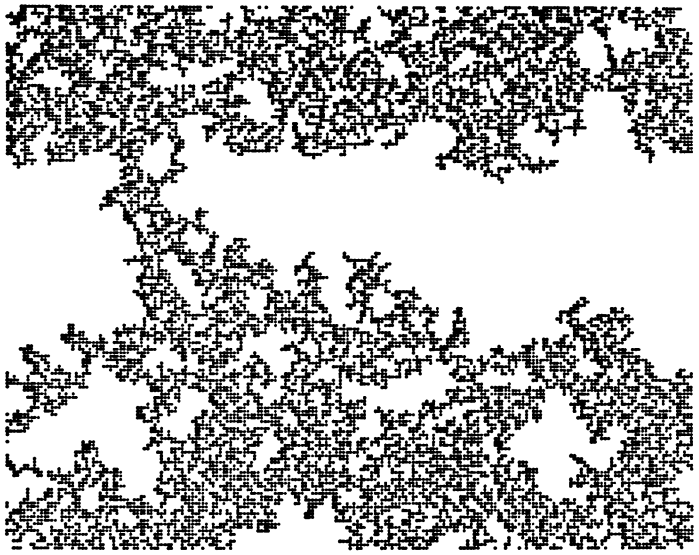

Fig. 2. A percolation cluster. Here 59.3% of the points of a square lattice are "occupied" (the rest are empty). Only the points that belong to the connected ("percolating") giant cluster are shown. This aggregate is a "random fractal" with $d_f = 1.896$ (= 91/48) and $d_s = 1.333$ (= 4/3).

Fractals (*6*) are objects with "fractal dimensions." There are many definitions of dimensions (*6–10*). For instance, for Fig. 2, on the average the mass of ink (or number of dots) in a box of radius r is proportional to r^{d_f}, where $d_f = 1.89$ (in contrast to $d_f = 2$ for a regular 2-D lattice). This percolation cluster is an example of a "random fractal." An example of an ordered fractal is given in Fig. 3. Here $d_f = (\log 3)/(\log 2) = 1.58$. Ordered fractals on the molecular level may not occur in nature. Actually, the random alloy discussed above is the most ideal experimental fractal system. Its fractal aspects (and dimension) are preserved on the scale of 1 nm to 1 cm (that is, a factor of 10^7). The exciton reactions that are confined to this fractal matrix (*4, 5*) inspired the theoretical work, including extensive simulations, that resulted in the following picture.

Batch reactions. Both phenomenologically and theoretically,

$$k = k_1 t^{-h} \quad 0 \leq h \leq 1 \quad (t \geq 1) \quad (9a)$$

where k is the instantaneous rate coefficient (replacing K in Eqs. 3a and 4a). The term "coefficient" rather than "constant" must be used, because in general k depends on the time, whereas $k_1 \equiv k(t = 1)$ does not. However, in 3-D (homogeneous) space, for the A + A reaction, $h = 0$, and thus k is a constant, in agreement with the classical-kinetics result. If a system is made homogeneous by vigorous stirring, h again will equal 0. However, for diffusion-limited reactions that occur in fractal spaces, theory (and simulations) give $h > 0$ and hence a time-dependent k. We thus call the general form

of Eq. 9a fractal-like kinetics (for $h > 0$). Nevertheless, Eq. 9a is not limited to fractals, but applies in many other nonclassical situations. For instance, for an A + A reaction in one dimension (*2*), theory and simulations give $h = 1/2$. Also, for an A + B reaction on a square lattice (*3*), for very long times, $h = 1/2$. Typical values for fractal systems are near $h = 1/3$ (see Fig. 1). Actually, for A + A reactions, $h = 1 - d_s/2$ (*4, 5*), where d_s is the so-called spectral (or random-walk recurrence) dimension (*6, 10*) defined below. Note that Eq. 9a is an approximation that fails at very short times.

Fractals differ from Euclidean spaces not only in their typical "fractal" dimension d_f (*6*), but also in having more than one relevant dimension. The "spectral dimension" is defined by the recurrence probability P of a random walker, that is, the probability of a random walker to return to its origin after time t:

$$P \sim t^{-d_s/2} \tag{10}$$

For Euclidean spaces, $d_s = d_f = d$. However, for fractal spaces, $d_s < d_f < d$ [where d is the dimension of the Euclidean space in which the fractal is embedded (*6*)]. For instance, for the Sierpinski gasket (Fig. 3) $d_s = 1.36$, whereas $d_f = 1.58$, and for the percolating cluster (Fig. 2) $d_s = 1.33$, whereas $d_f = 1.89$. Thus for the A + A reaction on a Sierpinski gasket, one expects from theory that $h = 1 - d_s/2 = 0.32$. Simulations reproduce this result (*4*). Similarly, for the percolating cluster, $h = 1 - d_s/2 = 0.33$, which has again been borne out (*4*) by simulations as well as by experiment (see above). Note here that for the whole class of random fractals, in all embedded Euclidean dimensions (two, three, or higher) d_s is always (*4, 10*) ~4/3 and thus $h = 1 - d_s/2 = 1/3$ for A + A reactions.

Steady-state reactions. A genuine "steady state" is time-independent by definition. The fractal-like nature expresses itself in an anomalous reaction order X. For instance, for the bimolecular A + A reaction,

$$\text{Rate} = K[\text{A}]^X \tag{11}$$

so that one finds (*4*) for the diffusion-limited case:

$$X = 1 + 2/d_s = 1 + (1 - h)^{-1} \quad (d_s < 2) \tag{11a}$$

Thus expected values are $X = 2.46$ for the Sierpinski gasket, $X = 2.5$ for the percolating cluster, and $X = 3$ for the 1-D A + A reaction! These results have been confirmed by Monte Carlo simulations (*4*). The mechanism of the reaction is still bimolecular. Although this would be an assumption for real experiments, it is built into the simulations (and shows the benefits of simulations, in that one can get anomalous orders from a simple bimolecular elementary step).

Clusters and islands. According to Mandelbrot (*6*, p. 1) there are "connected fractals" and there is "dust." The effective dimensions of "dust" are between zero and unity. A simple example of fractal dust is the Cantor set. Catalytic islands on noncatalytic supports are practical examples of "dust." Whether such "dust" is strictly fractal or is just made of monodisperse islands, the result is anomalous, fractal-like reaction kinetics. For fractal dust, with $0 < d_s < 1$, Eq. 11 results in $3 < X < \infty$, that is, anomalously large values of the reaction order X. For various finite clusters, lattice animals (*7, 8*) and monodisperse islands (square and linear), computer simulations (*9*) have indeed given unbelievably large X exponents (from 3 to 75). Historically, the first indication for such anomalously high reaction orders came from experiments (*5*). Semantically, any binary reaction kinetics with $h > 0$ or $X > 2$ are referred to as "fractal-like kinetics." Thus any surface diffusion-controlled reaction that occurs on clusters or islands is expected to be anomalous and fractal-like.

Segregation of reactants. Possibly the most dramatic manifestation of fractal-like reactions is the "spontaneous" segregation of reactants in A + B reactions, as had been predicted by Zeldovich and collaborators (*11*) and illustrated in simulations by Toussaint and Wilczek (*3*).

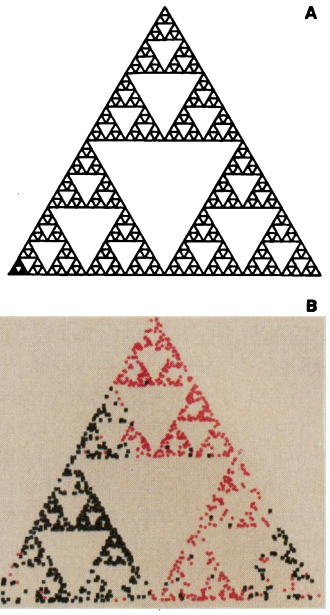

Fig. 3. (**A**) A Sierpinski "gasket." The density ρ of lattice points (vertices) as a function of base length (R) is given by $\rho = cR^{d_f}$, where c is a constant. Here the fractal dimension is $d_f = \log 3/\log 2 = 1.585$. The spectral dimension is $d_s = 1.365$. For a similar triangle without holes, $\rho = cR^{d_f}$, where $d_f = D = 2$; the spectral dimension is also $d_s = D = 2$. For further discussion, see (*6*). (**B**) A steady-state realization of the reaction A + B → AB↑ on a Sierpinski gasket. In this supercomputer simulation [von Neumann Center, Princeton (*12*)] there is a steady rate of A (red) and B (black) particles (equal amounts) landing at random locations on this fractal surface, then moving in random directions, a step at a time. When particle A steps on particle B (or B on A), both are annihilated (leave the surface). The very segregated realization shown is a snapshot taken after 1 million time steps. Landing rate: four pairs per time step. Note that the underlying lattice (left) is not shown here.

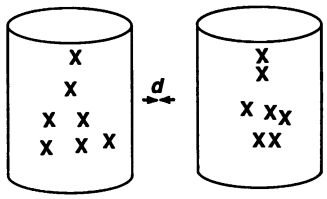

Fig. 4. Two identical "fractal" containers, with identical concentrations of reacting molecules, but with different instantaneous reaction rates. The probability for instantaneous reaction is obviously higher in the container on the right.

With absolutely no stirring, and a randomly prepared "batch" distribution of A and B reactants, one finds after a long time that the reactants segregate. Interestingly enough, although these reactions were run on Euclidean spaces (cube and square), the chemical kinetics at the time of segregation is fractal-like, for example, $h = 1/2$ for a square lattice (see above). This result is not surprising, as the reaction now proceeds in a lower dimensional space—the boundaries of the segregated domains [note that there is no relation between the Zeldovich effect and the Belusov-Zhabotinski reactions (*8*)].

Under steady-state conditions, no significant segregation is found in 2-D and 3-D Euclidean spaces (*12, 13*). However, for dimensions less than 2, a very striking segregation is observed (*12*) (Fig. 3B). Moreover, whereas for batch reactions the segregation only appears after a long time (when the reactant concentrations approach zero), for steady-state reactions the segregation occurs at both low and high concentrations.

The Meaning of Fractal-Like Kinetics

The replacement of the rate constant by a time-dependent rate coefficient $k(t)$ has unexpected consequences. Assume that one can look at one container with a batch reaction A + A → A_2↑ in progress, with instantaneous concentration [A] at time $t = 16$ s after preparation. Imagine another container that simultaneously happens to pass through the same instantaneous concentration [A], but being at time $t = 1$ s after its preparation. The second container obviously was prepared with a lower initial concentration, but both have the same concentration at observation time. Both containers are also assumed to have exactly the same thermodynamic conditions of temperature, pressure, and so forth. Thus they should react

Table 1. *F* factors (rounded).

Cubic lattice	1
Sierpinski gasket	2.5
Percolation cluster	4
Linear lattice	8
Linear islands (20 sites each)	18

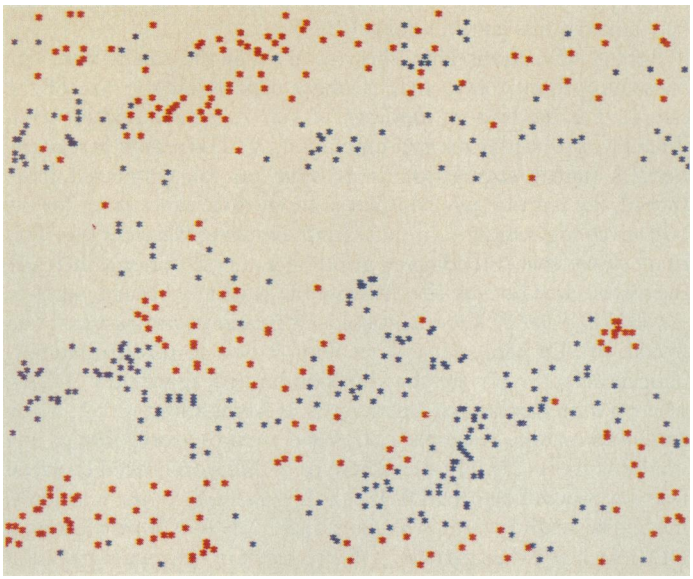

Fig. 5. A steady-state realization of the $A + B \rightarrow AB\uparrow$ reaction on a percolating cluster (Fig. 2) from a supercomputer simulation [San Diego Center (*9*)]. Landing rate: one pair per two steps. Other conditions are the same as in the caption of Fig. 3B. Note that the underlying lattice (Fig. 2) is not shown here.

classically at the same rate. However, with a fractal-like kinetics, this is not true. Assume that $h = 1/2$. For the first container $k = k_1 16^{-1/2} = k_1/4$, whereas for the second $k = k_1 1^{-1/2} = k_1$. At the time of observation, the second container is reacting with an instantaneous rate four times greater than the first one. How is this so?

One approach to the above dilemma is to say that the containers have a different history. The first was prepared longer ago and with a higher initial concentration. The passage of time has "degraded" the rate coefficient k. If these were real reactions, happening on a catalyst, we would have probably said that the catalyst got "poisoned." However, there is no "poison" in the computer simulations. There is also no reason to believe that poisoning occurs in the laboratory reactions studied (see below). What then is the difference between the two containers?

In specifying a concentration or a density for a noncrystalline thermodynamic system, one implicitly assumes a uniformly random distribution in space. Only under such an assumption can one expect that two systems with identical conditions will have identical reaction rates. Apparently, this is no longer true for our fractal containers. A simple example is given in Fig. 4. Obviously, for a bimolecular reaction to occur, two molecules must "pair up." We can measure such pairing-up in a number of ways. One simple method is to define a pair with the help of a maximum distance d (if the molecules are closer than d, they count as a pair). We can then define an instantaneous-reactivity criterion r to be given by the fraction of molecules included in such "pairs." For instance, in Fig. 4, $r = 6/7$ for the right-hand container, but $r = 0$ for the left-hand container. Note that a random distribution will eventually include pairs, whereas an ordered distribution, which looks like a lattice or a grid, will not. Although in a classical reaction system the distribution stays uniformly random, in a fractal-like reaction system the distribution tends to become "less random," that is, it is actually more ordered. A "mathematical" poisoning is thus created through self-ordering (see below). This effect is related to the compactness of low-dimensional random walk (*14, 15*).

A second reflection on the above example may lead to the conclusion that a fractal-like reaction might be more intuitive than a classical one. As pairs react ($A + A \rightarrow A_2\uparrow$), they are depleted. In time the fraction of pairs is reduced. However, in the classical case the ensemble manages to "rerandomize" itself (without stirring) and thus to keep up the supply of pairs. Hence the key question is: Can "self-stirring" compensate for pair depletion in a diffusion-limited reaction? It is at this point that the topology of the reaction space enters. In low dimensions a random walker is likely to stay at its original vicinity (*14*) and will eventually recross its starting point. In higher dimensions ($D > 2$) the random walker has a finite "escape probability" and may never return to the starting point. Thus a fractal-like kinetics is a "compact" kinetics (*15*)—the random walkers mostly "oscillate" around their original positions.

Importance of Initial Conditions

From our previous discussion it is apparent that initial conditions, which are usually of little importance in the "rerandomizing" classical kinetics, may be very important in fractal kinetics.

Batch versus steady-state creation and recombination. When the reactants A are produced suddenly (for example, photochemically by an intense but short laser pulse), one assumes that their distribution is random. However, when the reactants are produced at a steady rate, leading to a steady-state condition (for example, photochemical excitation by a continuous light source), the distribution is partially ordered (*16, 17*). Based on computer simulations (*16, 17*) one gets a novel effect for fractal-like reaction media. However, for a 3-D, isotropic (cubic) medium, one gets the classical result.

A simple empirical criterion for partial order is given by the factor F

$$F = k_0^r/k_0^{ss} \tag{12}$$

where k_0^r is the initial ($t = 0$) rate coefficient for random creation and k_0^{ss} is the one for steady-state creation, defined for equal initial concentrations:

$$[A]_0^r = [A]_0^{ss} \tag{13}$$

Table 1 lists some typical F factors derived from simulations (*16, 17*). The very large values observed for these F factors demonstrate that the nonrandom steady-state distribution for fractals and low-dimensional geometries manifests itself in extremely reduced reaction probabilities. Thus F is an "order parameter," because steady-state conditions in low-dimensional media are achieved only after a process of self-ordering. Specifically, for a 1-D lattice, the steady-state population has a quasi-periodic distribution, that is, it forms a quasi-superlattice, rather than a random, Poissonian distribution. Quantitatively, the nearest-neighbor distance (r) has a distribution $P(r)$ with a most probable value r_0 that defines a mesoscopic length scale, $r_0 >> a$, where a is the particle size (reaction cross section). Such a $P(r)$ distribution is also obtained at long times for batch reactions, irrespective of initial conditions (*18*). For instance, for $A + A \rightarrow A$, $P(r) \propto r \exp[-\beta(r - a)^2]$, where β is proportional to the reciprocal of the square of the particle density. Note that for a Poissonian distribution $P(r) \propto \exp[-\alpha(r - a)]$ and $r_0 = a$, where α is the reciprocal of the particle density.

Pair creation. Here we consider the reaction

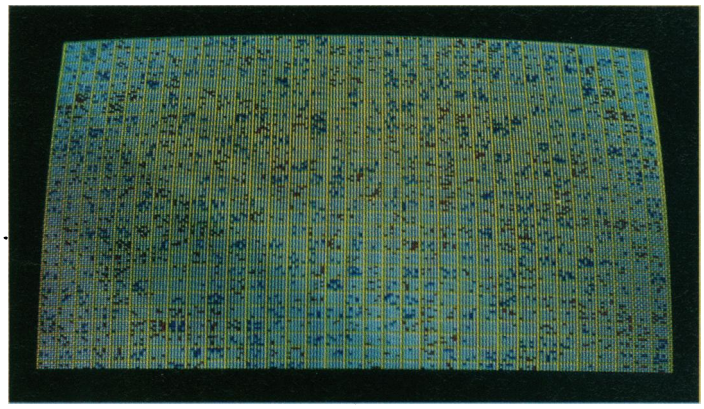

Fig. 6. A steady-state realization on an ensemble of monodisperse islands (5 by 5 sites) from a supercomputer simulation [San Diego Center (*9*)]. Snapshot after 5×10^5 steps. Landing rate: one pair per eight time steps.

Fig. 7. The shredding effect. The reaction $A + B \rightarrow AB\uparrow$ proceeds only on the rims of the surfaces. There is equal length of rim in both cases. The reaction $A + B \rightarrow AB\uparrow$ results in a higher steady-state density (lower reaction rate) for the connected catalyst (top), compared with the disjointed one (bottom).

$$A_2 \rightarrow A + A \rightarrow A_2\uparrow \qquad (1a)$$

We assume a catalytic surface onto which A_2 molecules land at random and immediately dissociate into A atoms. The atoms diffuse and react, giving a product (A_2) that immediately leaves the surface. A very drastic effect can be seen for a 1-D surface. Whereas a steady random landing of A atoms results in a steady-state reaction with a reaction order $X = 3$, according to Eq. 11a, a pairwise landing process gives $X = 2$ at steady state (*13, 18*). The pairwise landing process prevents the formation of a self-ordered steady state, resulting instead in a Poissonian steady state. This is an example of a subtle but important distinction that also applies for fractal surfaces. Note that Eq. 1a describes an equilibrium as well as a steady-state process. Maxwell's postulate ascribes a random (Poissonian) distribution to all kinetic equilibria.

Segregation and Self-Ordering

The self-ordering effect is much more prominent for the two-reactant (A + B) case. Focusing again on Fig. 3B (steady state), note that in this Monte Carlo simulation A and B particles land at random and move at random. When an A atom collides with a B (or B with A), the product AB desorbs. An A atom is not allowed to react with an A nor a B atom with a B. Thus A and B are created in pairs so that at all times [A] = [B] exactly. A drastic segregation such as in Fig. 3B happens for each computer realization, although the shape of the aggregates differs. Furthermore, segregation allows a much higher steady-state density compared with those in nonsegregated outcomes (*12*) (see below). No such steady-state segregation has been observed (*12*) for Euclidean spaces with dimension $d > 2$, nor is it expected theoretically (*19*).

A similar dramatic segregation effect is observed for random fractals, for example, a "percolating cluster" (see Fig. 5). As mentioned above, the underlying "lattice" (Fig. 2) itself has no apparent order. Nevertheless, the reactant distribution shows clear segregation of "unlike" particles and aggregations of "like" particles. However, these self-organization effects are no longer observed when all of the particles are allowed to react (that is, also allowing $A + A \rightarrow A_2\uparrow$ and $B + B \rightarrow B_2\uparrow$) or with pair creation. In the latter cases the particle distribution is random and the steady-state density is much lower (*9*). Segregation is also expected for most fractal media (where $d_s < 2$) and dispersed media (such as in Fig. 6).

Segregation and Wenzel's Law. Wenzel's law (1777) (*20*) states that for heterogeneous reactions, the larger the interface, the faster the reaction, that is, the rate per unit surface is constant. Except for obvious generalizations (only the "active" part of the surface should be counted), this law still holds (*21*).

Recent simulations have shown (*22*) that the steady-state rate constant, per unit area, may strongly depend on the size of the sample. For the bottom topology of Fig. 7, the reaction proceeds three times as fast as the top topology (*23*). The reason is segregation. A higher segregation is possible on the connected loop. Indeed, the reaction rate constant is about three times faster for the bottom configuration (*22*), thus clearly violating Wenzel's law. This result shows that shredding or grinding a sample not only increases the surface area but can also increase the reactivity per unit surface.

Clouds and colloids. Clouds, colloidal formations, and dust are often fractals (*6*). Of particular interest with respect to possible biomorphogenesis (*24, 25*) are the diffusion-limited aggregates (DLA), where a diffusion-limited kinetic process forms a fractal (*26*). Many natural formations resemble a DLA and are presumably formed in a similar fashion (*27*). We focus here on a diffusion-limited chemical reaction proceeding on a DLA. For $A + A \rightarrow A_2\uparrow$, the reaction is fractal-like with $h \cong 1/3$ (*28*). Presumably an A + B reaction on a DLA (such as a dust particle) will also result in reactant segregation and self-organization.

The origin of charge separation in colloids and clouds may also be attributed to reactive segregation. Ions randomly accreted by a colloid or cloud result in partial charge segregation (see Figs. 3B and 5) even without any external field. In addition, this effect is significantly amplified in the presence of a relatively weak field (Fig. 8). Much higher fields are required for nonreactive charge separation.

Experimental Fractal-Like Reactions

Photochemical and photophysical experiments with reaction

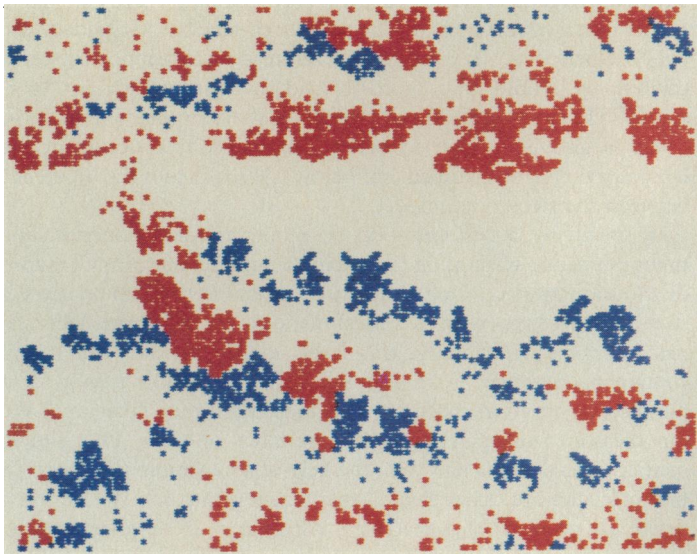

Fig. 8. Electric field effects on steady-state reactions. Same conditions as for Fig. 5, except for a directional bias influencing the random walk. In this supercomputer simulation [San Diego Center (*9*)], the snapshot is after 10^5 steps, and the direction bias is 0.35 to 0.15.

mechanisms known to be elementary, in cases where both product and reactant are easily followed in time, have served as ideal tests for fractal-like kinetics. Other systems besides excitons (see above) have been studied and are presented here.

Naphthalene photodimerization in porous membranes. The photodimerization of anthracene in solution was probably the first well-studied diffusion-limited reaction (*29*). The bimolecular reaction $A + A \rightarrow A_2$ (A = anthracene) followed the classical kinetics laws. A similar reaction provided the first study of fractal chemical kinetics:

$$N^* + N^* \rightarrow N_2^{**} \rightarrow N + N + \text{a photon} \qquad (16)$$

Here N* is a naphthalene molecule excited to its first triplet state and N_2^{**} is the transitory dimer in the first excited singlet state (*30, 31*). The experiment is performed in a solution embedded in various porous membranes [nylon (see Fig. 9) and acetate]. The naphthalene molecules diffuse inside the solvent inside the pores. A fractal-like kinetics with h on the order of 1/3 was obtained for the various membranes, whereas classically one expects $h = 0$.

Photophysical reaction in a 1-D fractal-like system. It has been mentioned that an A + A reaction in a 1-D system is fractal-like with $h = 1/2$. How thin a tube is necessary to have 1-D behavior? Simulations (*18*) show that if the reaction time is much longer than the time it takes the particles to reach the wall, then the reacting ensemble "knows" that it is confined to a 1-D medium.

To test this idea, a range of cylindrical tubes was used, with radii between 5 and 6000 nm. The tubes (Fig. 10) were channel pores in polycarbonate porous membranes. They were filled with crystalline naphthalene ($C_{10}H_8$ only) and exciton kinetics were studied (see Eq. 8). For the 100-nm and thicker naphthalene "wires" (*32*), $h = 0$, that is, classical kinetics held, as expected. For the very thin wires (<25 nm), the result was $h = 0.49$. Note that $h = 1/2$ is expected for 1-D systems. Thus 1-D structures with intermediate thickness exhibited fractal-like behavior ($0 < h < 1/2$), similar to the fractal behavior of the percolation cluster ($h = 1/3$) described earlier.

These 1-D wires have also been subjected to the initial condition tests (see above). The thinnest wires showed a factor $F \approx 5$ (see Eq. 12), whereas the thickest ones showed $F = 1$. This result is consistent with those in Table 1. [In addition, preliminary experiments on solution photodimerization of naphthalene inside the thinnest cylindrical pores gave $h = 0.4 \pm 0.1$, in good agreement with the expected theoretical value and the above exciton experiments.]

Applications of Fractal Kinetics

Fractal kinetics as a structural tool. Porous glass (Vycor) has recently been under active investigation, because of a controversy (*31–33*) about its pore topology: is it fractal, like a percolation cluster (Fig. 1), or is it effectively one dimensional? Porous glass has been subjected (*16, 31, 32*) to two fractal-kinetics tests as was done for exciton fusion in naphthalene-embedded pores: (i) the h value and (ii) the F factor. Both tests support the nonfractal topology. Similar tests have been performed on a number of composites containing porous polymeric membranes and filter papers (*31*). Also, the domain-boundary topology of vapor-deposited films has been investigated (*4, 34*), as well as the effective topology of molecular clusters in molecularly doped polymers (*4, 35*) and the chain topology in dilute polymeric blends (*36*). In all of these cases consistent results were obtained. More such applications can be envisioned, such as the investigation of surfaces of catalysts, electrodes, and electronic devices.

Fractal kinetics as a tool for reaction kinetics. The major goal of this work is to understand heterogeneous reaction kinetics in areas such as chemistry, biology, geology, solid-state physics, astrophysics, and atmospheric sciences. Only the first steps have been taken in this direction, such as energy transport studies in condensed phases (*37*) and the dimerization and recombination studies mentioned above. Although the molecular kinetics experiments (*30*) may be viewed as preliminary evidence, the exciton-kinetics experiments (*4, 5, 9, 31, 32, 34–38*) have given consistent results in different laboratories for more than a decade. Note that even the presence of partial convection may still leave a surprising degree of "understirring," especially in low dimensions (*39–41*).

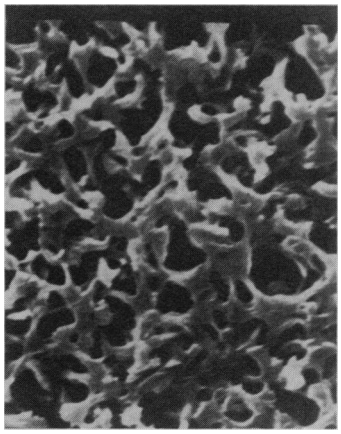

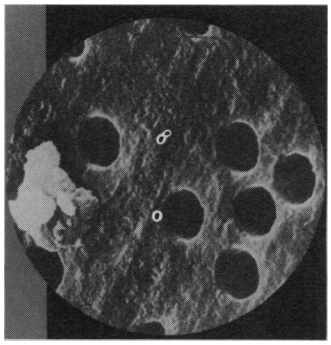

Fig. 9 (left). Porous nylon membrane (Gelman, Ann Arbor, Michigan). Magnification about $\times 10^4$. **Fig. 10 (right).** Channel-pore polycarbonate membrane (Nuclepore, Pleasanton, California). Magnification about $\times 10^4$. Thickness, ~6 μm.

Summary

Diffusion-controlled reactions with geometrical constraints, as found in heterogeneous kinetics, may be described by reactions on fractal domains. The hallmarks of "fractal-like" reactions are anomalous reaction orders and time-dependent reaction rate "constants." These anomalies stem from the nonrandomness of the reactant distributions in low dimensions. For homo-bimolecular reactions ($A + A \rightarrow Pr$) the distribution is partially ordered, for example, quasi-periodic. However, for hetero-bimolecular reactions ($A + B \rightarrow Pr$) the reactants segregate. Theory, simulations, and experiments are interrelated through the formalism of fractal reaction kinetics (*42*).

REFERENCES AND NOTES

1. M. V. Smoluchowski, *Z. Phys. Chem.* **92**, 129 (1917); J. Keizer, *J. Phys. Chem.* **86**, 5052 (1982), and references therein.
2. D. C. Torney and H. M. McConnel, *J. Phys. Chem.* **87**, 1441 (1983).
3. D. Toussaint and F. Wilczek, *J. Chem. Phys.* **78**, 2642 (1983).
4. R. Kopelman, *J. Stat. Phys.* **42**, 185 (1986), and references therein.
5. P. Klymko and R. Kopelman, *J. Phys. Chem.* **86**, 3686 (1982); *ibid.* **87**, 4565 (1983).
6. B. B. Mandelbrot, *The Fractal Geometry of Nature* (Freeman, San Francisco, 1983).
7. D. Stauffer, *Introduction to Percolation Theory* (Taylor and Francis, London, 1985).
8. J. Rudnick and G. Gaspari, *Science* **237**, 384 (1987); C. Grebogi, E. Ott, J. A. Yorke, *ibid.* **238**, 632 (1987).
9. J. S. Newhouse and R. Kopelman, *J. Chem. Phys.* **85**, 6804 (1986); *J. Phys. Chem.* **92**, 1538 (1988).
10. S. Alexander and R. Orbach, *J. Phys. (Paris) Lett.* **43**, L625 (1982).
11. A. A. Ovchinikov and Ya. B. Zeldovich, *Chem. Phys.* **28**, 215 (1978), and references therein; V. N. Kuzovkov and E. A. Kotomin, *J. Phys. C* **17**, 2283 (1984).
12. L. W. Anacker and R. Kopelman, *Phys. Rev. Lett.* **58**, 289 (1987); *J. Phys. Chem.* **91**, 5555 (1987).
13. L. Li and R. Kopelman, *J. Lumin.* **40/41**, 688 (1988).
14. S. Chandrasekhar, *Rev. Mod. Phys.* **15**, 1 (1943).
15. P. G. de Gennes, *J. Chem. Phys.* **76**, 3316 (1982).
16. R. Kopelman, L. Li, S. J. Parus, J. Prasad, *J. Lumin.* **38**, 289 (1987).
17. R. Kopelman and S. J. Parus, in *Fractal Aspects of Materials*, D. W. Schaefer, R. B.

Laibowitz, B. B. Mandelbrot, S. H. Liu, Eds. (Materials Research Society, Boston, 1986), vol. 2, pp. 50–52; R. Kopelman *et al.*, *Chem. Phys.*, in press.
18. L. Li and R. Kopelman, unpublished results.
19. K. Lindenberg, B. J. West, R. Kopelman, *Phys. Rev. Lett.* **60**, 1777 (1988).
20. C. F. Wenzel, *Lehre von der Verwandtschaft der Körper* **8** (Dresden, 1777).
21. D. Farin and D. Avnir, *J. Phys. Chem.* **91**, 5517 (1987). Note that when one grinds the material in order to speed up the reaction, this is simply a way of increasing the surface. It is not related to the connectedness or disjointedness of the reactive surfaces.
22. E. Clement and R. Kopelman, unpublished results.
23. Note that the reaction occurs only on the rims (black lines) and that there is equal length of rim in both cases.
24. A. M. Turing, *Philos. Trans. R. Soc. London Ser. B* **237**, 37 (1952); see also R. J. Field, *Am. Sci.* **142** (1985).
25. J. Maddox, *Nature* **326**, 327 (1987).
26. T. A. Witten and L. M. Sander, *Phys. Rev. Lett.* **47**, 1400 (1981).
27. L. M. Sander, *Sci. Am.* **255**, 94 (January 1987).
28. L. M. Sander, private communication.
29. R. Luther and F. Weigert, *Z. Phys. Chem.* **53**, 385 (1905).
30. J. Prasad and R. Kopelman, *J. Phys. Chem.* **91**, 265 (1987). As in Eq. 16, the second step is a million times faster, and the reaction rate can be monitored by the ultraviolet light. There is also a slow side-reaction where the triplet state emits a green photon. The instantaneous reactant concentration is thus monitored in time by green light, while the reaction (fusion) is monitored by ultraviolet light.
31. R. Kopelman, S. Parus, J. Prasad, *Phys. Rev. Lett.* **56**, 1742 (1986).
32. J. Prasad and R. Kopelman, *ibid.* **59**, 2103 (1987). It is also known (*31*) that the "cruising range" of the triplet excitons is about 100 nm (and somewhat dependent on temperature). Intermediate thicknesses give intermediate *h* values. The crossover from 1-D to 3-D behavior is at a radius corresponding to the excitation "cruising range" (actually a more precise cruising range can be obtained from these data). Even the temperature effect is as expected—the hopping rate increases somewhat with temperature.
33. D. W. Schaefer, B. C. Bunker, J. P. Wilcoxon, *ibid.* **58**, 284 (1987); U. Even, K. Rademann, J. Jortner, N. Manor, R. Reisfeld, *ibid.*, p. 285.
34. L. A. Harmon and R. Kopelman, *J. Lumin.* **31/32**, 660 (1984).
35. E. I. Newhouse and R. Kopelman, *Chem. Phys. Lett.* **143**, 106 (1988).
36. C. S. Li and R. Kopelman, unpublished results.
37. A. Blumen, J. Klafter, G. Zumofen, in *Optical Spectroscopy of Glasses*, I. Zschokke, Ed. (Reidel, Dordrecht, 1986), p. 199.
38. P. Evesque and J. Duran, *J. Chem. Phys.* **80**, 3016 (1984).
39. Y. Luo and I. R. Epstein, *ibid.* **85**, 5733 (1986).
40. J. C. Roux, P. De Kepper, J. Boissonade, *J. Phys. Lett.* **A97**, 168 (1983).
41. P. Argyrakis and R. Kopelman, *J. Phys. Chem.*, in press.
42. Supported by NSF grant DMR 8303919, PRF grant 18791-AC5, 6 and NSF Special Supercomputer Allocations at the John von Neumann National Supercomputer Center and the San Diego Supercomputer Center.

Developmental Regulation of Two 5*S* Ribosomal RNA Genes

ALAN P. WOLFFE* AND DONALD D. BROWN

The developmental regulation of two kinds of *Xenopus* 5*S* RNA genes (oocyte and somatic types) can be explained by differences in the stability of protein-protein and protein-DNA interactions in a transcription complex that directs transcription initiation by RNA polymerase III. Dissociation of transcription factors from oocyte 5*S* RNA genes during development allows them to be repressed by chromatin assembly. In the same cells, somatic 5*S* RNA genes remain active because their transcription complexes are stable.

THE FROG *XENOPUS LAEVIS* CONTAINS TWO KINDS OF multigene families that encode 5*S* ribosomal RNA, an essential component of ribosomes. *Xenopus* oocytes synthesize and accumulate large amounts of 5*S* RNA encoded for by a large multigene family called oocyte 5*S* DNA. Oocytes also express a small multigene family (somatic 5*S* DNA). After fertilization and development of the embryo, the oocyte-specific 5*S* RNA genes are repressed, while the somatic 5*S* RNA genes remain active. This is an example of what may be a common developmental mechanism: where two (or more) gene families have similar (but not identical) cis-acting controlling elements that are recognized by the same factors but are nonetheless controlled differently. In studying the developmental control of this "dual" 5*S* RNA gene system, we have sought to understand the molecular mechanisms that establish and maintain this pattern of differential gene activity.

The authors are in the Department of Embryology at the Carnegie Institution of Washington, 115 West University Parkway, Baltimore, MD 21210.

*Present address: Laboratory of Molecular Biology, National Institute of Diabetes and Digestive and Kidney Diseases, National Institutes of Health, Bethesda, MD 20892.

The 5*S* RNA Genes of *Xenopus laevis*

The structure and organization of the three kinds of 5*S* RNA genes that have been characterized from the *X. laevis* genome are diagrammed in Fig. 1. These are called major oocyte (*Xlo*) (*1*), trace oocyte (*Xlt*), and somatic (*Xls*) 5*S* DNA (*2*). Each class is organized in clusters of simple tandem repeats. All three classes are transcribed in growing oocytes, while somatic 5*S* DNA transcription contributes more than 95% of the 5*S* RNA synthesized in somatic cells (*3*). Because there are only 400 somatic 5*S* RNA genes but over 20,000 oocyte 5*S* RNA genes per haploid genome, this is a final differential gene transcription of over 1000-fold in somatic cells. We refer to this as a somatic-to-oocyte ratio (S/O) of 1000. The two kinds of oocyte-specific 5*S* RNA genes (*Xlt* and *Xlo*) are similar enough that we will concentrate on the differential transcription of *Xlo* and *Xls* 5*S* RNA genes in this article. There are six nucleotide differences between *Xlo* and *Xls* 5*S* RNA genes (Fig. 1), and the spacers are completely different except for short conserved elements near the 5′ and 3′ ends of the gene. We assess the importance of these sequence differences by in vitro (*4*) and in vivo (*5*) transcription assays, where full-length 5*S* RNA is synthesized.

The 5*S* RNA genes are accurately and efficiently transcribed by RNA polymerase III when they are injected into oocyte nuclei or incubated in extracts of these same nuclei. Transcription initiation is